Speed-Up Technique of Extended Boundary Node Method for Large-Scale Simulation[*]

Ayumu SAITOH, Atsushi KAMITANI[1] and Hiroaki NAKAMURA[2]

University of Hyogo, 2167 Shosha, Himeji, Hyogo 671-2280, Japan
[1]*Yamagata University, 4-3-16 Johnan, Yonezawa, Yamagata 992-8510, Japan*
[2]*National Institute for Fusion Science, 322-6 Oroshi-cho, Toki, Gifu 509-5292, Japan*

The eXtended Boundary Node Method (X-BNM) with the periodic Radial Point Interpolation Method (RPIM) shape function is proposed and its performance is investigated numerically. The results of computations show that the accuracy of the X-BNM with the periodic RPIM shape function is almost equal to that with the Moving Least-Squares (MLS) shape function. In addition, the speed of the X-BNM with the periodic RPIM shape function is extremely faster than that with the MLS shape function. Therefore, the periodic RPIM shape function is useful for improving the performance of the X-BNM.

1. Introduction

The boundary element method (BEM) is a numerical method for solving boundary-value problems of partial differential equations and has been so far used in the field of the nuclear fusion science. For example, the BEM has been adopted to solve the Grad-Shafranov equation which describes the magnetohydrodynamics equilibrium of plasma in terms of the poloidal magnetic flux [1]. Although the BEM is well suited for solving the Grad-Shafranov equation, it has the inherent demerit: a boundary must be divided into a set of elements before executing the BEM code.

In order to resolve the above demerit, Mukherjee *et al.* developed the boundary node method (BNM) [2]. Because the BNM is one of the meshless approaches, the preparation of the input data can be extremely simplified. In addition, the BNM has been reformulated without using integration cells and its performance has been investigated numerically [3, 4]. This method is called the extended BNM (X-BNM). The results of computations show that the accuracy of the X-BNM is much higher than that of the dual-reciprocity BEM. In addition, we have modified the X-BNM for enhancing the accuracy degradation due to the complex boundary shape [5].

In spite of a high usefulness, the X-BNM has the following demerit. The shape function lacks the Kronecker delta function property. This causes that the number of unknowns is equal to twice that of boundary nodes. On the other hand, Wang and Liu proposed the radial point inter-

polation method (RPIM) [6]. The RPIM has the advantage that the shape function possesses the Kronecker delta function property. If the shape function used in the RPIM were applied to the X-BNM, the demerit for the speed of the X-BNM could be removed.

In previous works, we proposed an acceleration technique for the X-BNM by applying the RPIM shape function. The results of computations have showed that the speed of the X-BNM with the RPIM shape function is extremely faster than that with the Moving Least-Squares (MLS) shape function [7]. However, the accuracy of the proposed method is drastically degraded because of the lack of periodicity of the shape function.

The purpose of the present study is to numerically investigate the performance of the X-BNM with the periodic RPIM shape function.

2. Function Interpolation

In the X-BNM, both a solution u and its normal derivative $q \equiv \partial u / \partial n$ are assumed to be contained in the functional space $V \equiv \mathrm{span}\,(\Phi_1, \Phi_2, \cdots, \Phi_N)$ where the shape function $\Phi_i(s)$ is a function of the arclength s along the boundary. Hence, $\Phi_i(s)$'s must be determined by using arclengths assigned to boundary nodes. In this study, we summarize the two approaches for deriving the shape functions.

2.1 Shape function

The approximate function $f^{\mathrm{h}}(s)$ of a function $f(s)$ can be written as

$$f^{\mathrm{h}}(s) = \boldsymbol{p}^T(s)\,\boldsymbol{a}(s), \tag{1}$$

where $p(s) = [p_1(s), p_2(s), \cdots, p_m(s)]^T$ is a monomial basis of order m and $a(s)$ is a m-dimensional vector such that all components are a function of s.

$a(s)$ can be determined by minimizing the following functional:

$$J[a(s)] \equiv \sum_{i=1}^{N} w_i(s) \left[p^T(s_i)\, a(s) - f(s_i) \right]^2,$$

where s_i and $w_i(s)$ denote the arclength to the ith boundary node and a weight function with a compact support, respectively. From the stationarity condition of the functional $J[a(s)]$ with respect to $a(s)$, we obtain

$$A(s)a(s) = B(s)f, \tag{2}$$

where $A(s)$, $B(s)$ and f are defined by

$$A(s) = \sum_{i=1}^{N} w_i(s)\, p(s_i)\, p^T(s_i),$$

$$B(s) = \sum_{i=1}^{N} w_i(s)\, p(s_i)\, e_i^T,$$

$$f = \sum_{i=1}^{N} f(s_i)\, e_i.$$

Here, $\{e_1, e_2, \cdots, e_N\}$ is the orthonormal system of the N-dimensional vector space.

By solving (2) and substituting it into (1), we can get

$$f^{h}(s) = \sum_{i=1}^{N} \Phi_i^{M}(s)\, f(s_i), \tag{3}$$

where

$$\Phi_i^{M}(s) = p^T(s)\, A^{-1}(s)\, B(s)\, e_i. \tag{4}$$

Throughout the present study, $\Phi_i^{M}(s)$ is called the MLS shape function. Note that the shape function $\Phi_i^{M}(s)$ fulfills $\Phi_i^{M}(s_j) \neq \delta_{i,j}$ where $\delta_{i,j}$ is the Kronecker's delta. This means that the number of unknowns is twice that of boundary nodes. In other words, the solution of the linear system obtained by the discretization does not become the value of either u or q on the boundary node. Therefore, the speed of the X-BNM is extremely lower than that of the mesh-based methods, e.g., the BEM.

In order to overcome the demerit of the MLS shape function, the interpolation technique used in the RPIM has been proposed. By using the radial basis function $r_i(s)$ and the monomial basis function $p_i(s)$, the shape function can be determined. Then, the curve passing through all boundary nodes is assumed as the approximate function. The approximate function $f^{h}(s)$ of $f(s)$ in the influence domain can be written as

$$f^{h}(s) = h_i(s) \left[r^T(s)\, b(s) + p^T(s)\, a(s) \right]. \tag{5}$$

Here, $h_i(s)$ is given by

$$h_i(s) = H\left(1 - |s - s_i| / R_i\right),$$

where $H(x)$ and R_i denote the Heaviside step function and the ith support radius, respectively. In addition, $r(s) = [r_1(s), r_2(s), \cdots, r_N(s)]^T$ is the set of radial basis functions and $b(s)$ is a N-dimensional vector such that all components are functions of s.

In order to determine $a(s)$ and $b(s)$, we enforce the interpolation to satisfy the given value at the boundary nodes as

$$\begin{bmatrix} R(s) & P(s) \\ P^T(s) & O \end{bmatrix} \begin{bmatrix} b(s) \\ a(s) \end{bmatrix} = \begin{bmatrix} f \\ 0 \end{bmatrix}, \tag{6}$$

where $R(s)$ and $P(s)$ are defined by

$$R(s) = \sum_{i=1}^{N} h_i(s)\, r(s_i)\, r^T(s_i),$$

$$P(s) = \sum_{i=1}^{N} h_i(s)\, e_i\, p^T(s_i).$$

By solving (6) and substituting it into (5), we can get

$$f^{h}(s) = \sum_{i=1}^{N} \Phi_i^{R}(s)\, f(s_i), \tag{7}$$

where

$$\Phi_i^{R}(s) = \left[r^T(s), p^T(s) \right] \begin{bmatrix} R(s) & P(s) \\ P^T(s) & O \end{bmatrix}^{-1} \begin{bmatrix} e_i \\ 0 \end{bmatrix}. \tag{8}$$

The shape function $\Phi_i^{R}(s)$ has the Kronecker delta function property. Therefore, the number of unknowns is equal to that of boundary nodes. In this study, $\Phi_i^{R}(s)$ is called the RPIM shape function.

2.2 Periodicity

When the length of the boundary denotes L, s becomes a periodic function of period L. In this sense, it is necessary for the shape functions have periodicity. However, the shape functions generated from the global arclengths, $s_1, s_2, \cdots, s_N$, do not have periodicity. In this study, we propose an algorithm to calculate the periodic shape function by using the following two steps:

1. $s_1^*, s_2^*, \cdots, s_N^*$ are determined by using the following equation: $s_j^* = \mathrm{mod}\left(s_j - (s - L/2), L\right) + s - L/2$.
2. The shape function is calculated on the basis of $s_1^*, s_2^*, \cdots, s_N^*$.

Let us investigate the behavior of the MLS shape functions and that of the RPIM one. In the numerical experiments, five nodes are uniformly placed on the boundary of a unit circle. In the MLS shape function, the spline-type weight function is assumed. The explicit form of the weight function is given by

$$w_i(s) = \omega\left(|s - s_i| / R_i\right),$$
$$\omega(r) = H(1 - r)(1 - 6r^2 + 8r^3 - 3r^4).$$

(a)

(b)
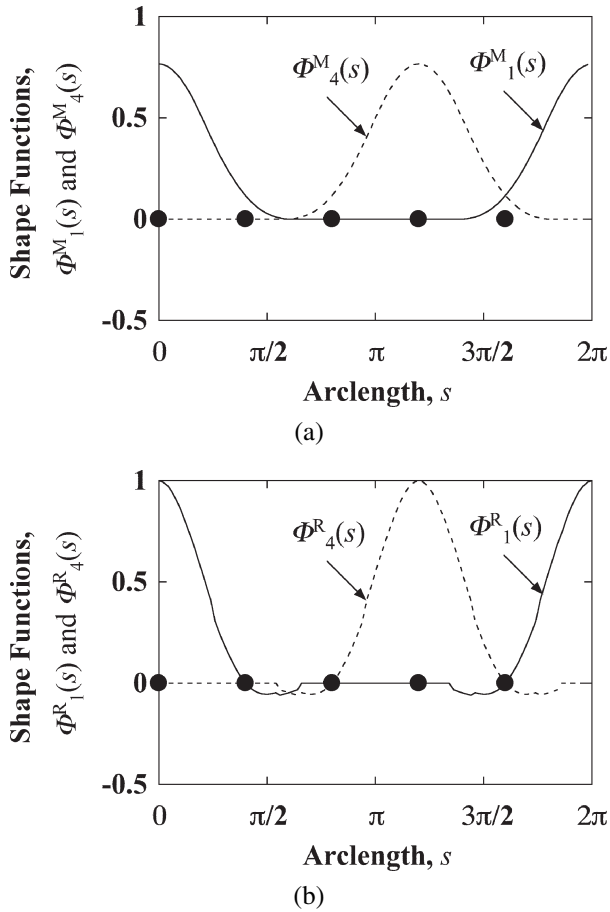
Fig. 1   (a) The behavior of the MLS shape functions and (b) that of the RPIM shape function. Here, the parameters are fixed as follows: $m = 2$ and $\gamma = 1.6$. The symbol • indicates the boundary node.

In the RPIM shape function, $r_i(s)$ is given by the compactly supported radial basis function (CSRBF) [8] and its explicit form is expressed as

$$r_i(s) = \rho\left(|s - s_i|/R_i\right),$$
$$\rho(r) = (1 - r)^3(3r + 1).$$

In both shape functions, R_i is defined by

$$R_i = \gamma \min\left(\left|s_{\bmod (i+1,N)} - s_i\right|, \left|s_{\bmod (i-1,N)} - s_i\right|\right),$$

where γ is a constant.

As a typical example, we compute the shape functions, $\Phi_i^M(s)$ and $\Phi_i^R(s)$, and show their behavior (Figs. 1 (a) and 1 (b)). We see from these figures that both shape functions are a smooth function with a period of 2π. Moreover, the MLS shape function lacks the Kronecker delta function property, whereas the RPIM shape function satisfies it.

From these results, we can completely remove the demerit of the MLS approximation by using the RPIM approximation.

3. Performance Evaluation

In this section, the performance of the X-BNM with

Table 1   Evaluation Environment.

Parameter	Value
OS	MacOS X 10.9
CPU	Intel Core i5 1.3 GHz
Memory	4 GB
Compiler	gfortran 4.8.2
Compiler option	-O3

the periodic RPIM shape function is investigated numerically. As an example problem, we adopt the 2-D Poisson problem over $\Omega \equiv \left\{(x, y) \left\| \left[x - \Delta(y/2)^2\right]^2 + (y/2)^2 < 1\right.\right\}$ and the given functions used in the 2-D Poisson problem are determined so that the analytic solution may be $u = e^{-3(x^2+y^2)} - \cosh x \sin y + \cos x \sinh y$. Also, only the Direclet problem is solved throughout the present study.

When the Poisson equation is transformed to an equivalent boundary integral equation, the equation contains not only the boundary integrals but also a domain integral. In order to remain only the boundary integrals, we assume that the right hand side $g(\boldsymbol{x})$ of the Poisson equation is approximated as

$$g(\boldsymbol{x}) = \sum_{l=1}^{M} \alpha_l \rho\left(\frac{|\boldsymbol{x} - \boldsymbol{x}_l|}{\bar{R}}\right), \tag{9}$$

where $\boldsymbol{x}_1, \boldsymbol{x}_2, \cdots, \boldsymbol{x}_M$ are poles on $\partial\Omega \cup \Omega$. Moreover, $\bar{R}$ and α_l's are all constants. Throughout the present study, $\bar{R}$ is fixed as $\bar{R} = 1.5$.

The more detail with respect to the discretization of the 2-D Poisson problem by means of the X-BNM can be found in [3]. In the following, the Gauss-Legendre quadrature with N_G is employed as the integration method and its value is fixed as $N_G = 12$. Moreover, the evaluation environment is shown in Table 1.

In our previous work, parameters used in the MLS shape function are fixed as $m = 1$ and $\gamma = 1$ [3]. Hence, we employ parameters of the RPIM shape function as is the case in the MLS shape function.

As the measure of the accuracy, we adopt the relative error defined by

$$\varepsilon = \frac{\sqrt{\left\|u_A - u_N\right\|^2 + \left\|q_A - q_N\right\|^2}}{\sqrt{\left\|u_A\right\|^2 + \left\|q_A\right\|^2}},$$

where the subscript notations, A and N, are analytic and numerical solutions, respectively, and $\| \; \|$ denotes the Euclidean norm. In this section, the X-BNM with the MLS shape function, the X-BNM with the conventional RPIM shape function and the X-BNM with the periodic RPIM shape function are called the X-BNM(MLS), the X-BNM(Conventional RPIM) and the X-BNM(Periodic RPIM), respectively.

Let us first investigate the accuracy of the X-BNM(Periodic RPIM). The relative errors are calculated
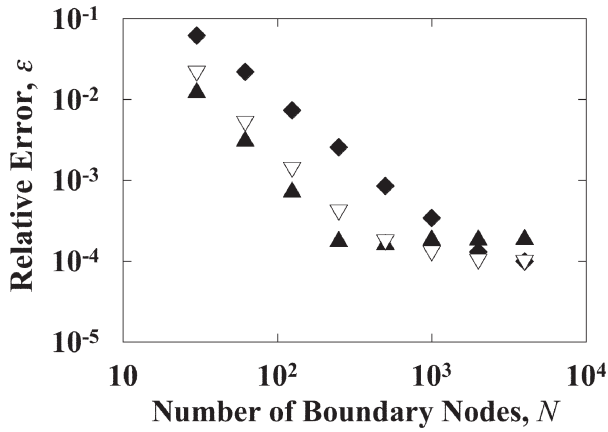
Fig. 2　Dependence of the relative error ε on the the number N of boundary nodes for the case with $\Delta = 0$. Here, the symbols, ▲, ♦ and ▽ denote the X-BNM(MLS), the X-BNM(Conventional RPIM) and the X-BNM(Periodic RPIM), respectively.
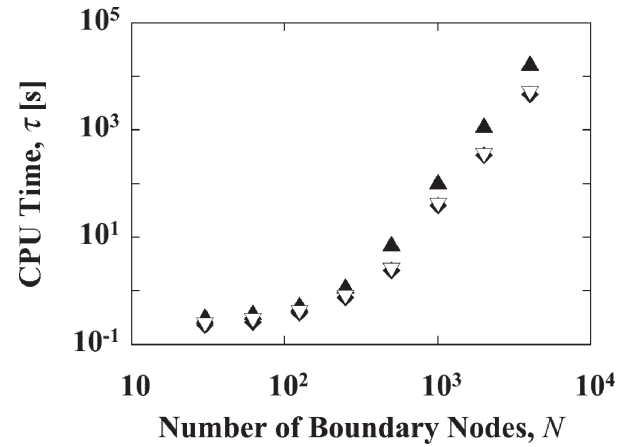
Fig. 4　Dependence of the CPU time τ on the the number N of boundary nodes for the case with $\Delta = 0$. Here, the symbols, ▲, ♦ and ▽ denote the X-BNM(MLS), the X-BNM(Conventional RPIM) and the X-BNM(Periodic RPIM), respectively.
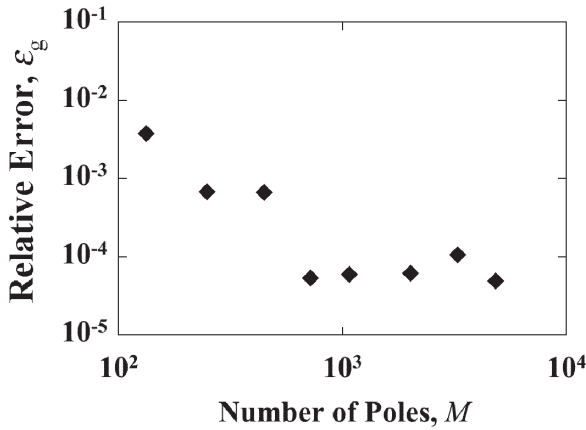
Fig. 3　Dependence of the approximation accuracy of (9) on the the number M of poles for the case with $\Delta = 0$.

Fig. 5　Dependence of the relative error ε on the triangularity Δ for the case with $N = 500$. Here, the symbols, ▲, ♦ and ▽ denote the X-BNM(MLS), the X-BNM(Conventional RPIM) and the X-BNM(Periodic RPIM), respectively.

as a function of N and are depicted in Fig. 2. We see from this figure that the accuracy of the X-BNM(Periodic RPIM) is higher than that of the X-BNM(Conventional RPIM). Moreover, the accuracy of the X-BNM(Periodic RPIM) is almost equal to that of the X-BNM(MLS). In addition, the relative errors of the X-BNM(MLS) and the X-BNM(Periodic RPIM) are saturated for $N \gtrsim 500$. In order to investigate this tendency in detail, we indicate the dependence of the approximation accuracy of $g(\boldsymbol{x})$ on the number M of the poles. As the measure of the approximation accuracy of $g(\boldsymbol{x})$, we adopt the relative error defined by

$$\varepsilon_{\mathrm{g}} = \frac{\left\| g(\boldsymbol{x}) - \sum_{l=1}^{M} \alpha_l \, \rho\left(\frac{|\boldsymbol{x} - \boldsymbol{x}_l|}{\bar{R}} \right) \right\|_{\infty}}{\| g(\boldsymbol{x}) \|_{\infty}},$$

where $\| \ \|_{\infty}$ denotes the maximum norm. The relative error ε_{g} is plotted as a function of M in Fig. 3. The relative error decreases with an increase in M, whereas it

almost becomes dominant with an increase in M for the case with $M \gtrsim 700$. This result shows that the limit of ε_{g} is almost equal to 10^{-4}. Therefore, relative errors of the X-BNM(MLS) and the X-BNM(Periodic RPIM) become constant for $N \gtrsim 500$ because the discretization error is smaller than the approximation error of $g(\boldsymbol{x})$.

Next, we evaluate the speed of the X-BNM(Periodic RPIM). The CPU times are plotted as a function of N in Fig. 4. This figure indicates that not only the speed of the X-BNM(Conventional RPIM) but also that of the X-BNM(Periodic RPIM) is faster than that of the X-BNM(MLS) for the case with $N \gtrsim 500$.

Finally, we investigate the influence of the triangularity Δ on the accuracy of the X-BNM(Periodic RPIM). To this end, the relative errors are calculated as a function of Δ and are plotted in Fig. 5. We see from this figure that relative errors of the X-BNM(MLS) and the X-BNM(Periodic

RPIM) increase with an increase in Δ. However, both the relative error of the X-BNM(Periodic RPIM) and that of the X-BNM(MLS) are much lower than that of the X-BNM(Conventional RPIM) regardless of Δ.

4. Conclusion

We have proposed the X-BNM with the periodic RPIM shape function so that the number of unknowns becomes equal to that of boundary nodes (i.e., the shape function has the Kronecker delta function property). In addition, its performance has been investigated numerically. Conclusions obtained in this paper are summarized as follows.

1. The accuracy of the X-BNM with the periodic RPIM shape function is almost equal to that with the MLS shape function. Even if the boundary shape is strongly concave, this tendency does not change.
2. The speed of the X-BNM with the periodic shape function is always faster than that with the MLS shape function for the case where the number of boundary nodes exceeds a certain limit.

From the above mentions, we might conclude that the X-BNM with the periodic RPIM shape function is a powerful method for a large-scale simulation. In the future work, we will apply the X-BNM with the periodic RPIM shape function to the problems of the field of the nuclear fusion science such as the boundary-value problem of the Grad-Shafranov equation.

[1] M. Itagaki and T. Fukunaga, Eng. Anal. Bound. Elem. **30**, 746 (2006).
[2] Y.X. Mukherjee and S. Mukherjee, Int. J. Numer. Meth. Eng. **40**, 797 (1997).
[3] A. Saitoh, S. Nakata, S. Tanaka and A. Kamitani, Information **12(5)**, 973 (2009) [in Japanese].
[4] A. Saitoh, N. Matsui, T. Itoh and A. Kamitani, IEEE Trans. Magn. **47(5)**, 1222 (2011).
[5] A. Saitoh, K. Miyashita, T. Itoh, A. Kamitani, T. Isokawa, N. Kamiura and N. Matsui, IEEE Trans. Magn. **49(5)**, 1601 (2013).
[6] J.G. Wang and G.R. Liu, Int. J. Numer. Meth. Eng. **54(11)**, 1623 (2002).
[7] A. Saitoh, T. Itoh, N. Matsui and A. Kamitani, IEEE Trans. Magn. **50(2)**, 7011404 (2014).
[8] C.S. Chen, C.A. Brebbia and H. Power, Commun. Numer. Meth. Eng. **15**, 137 (1999).